World Academy of Science, Engineering and Technology
International Journal of Chemical and Materials Engineering
Vol:13, No:7, 2019

Investigating the Formation of Nano-Hydroxyapatite on a Biocompatible and Antibacterial Cu/Mg-Substituted Bioglass

Elhamalsadat Ghaffari, Amirhossein Moghanian, Amir Khaleghipour

***Abstract*—**Multifunctional bioactive glasses (BGs) are designed with a focus on the provision of bactericidal and biological properties desired for angiogenesis, osteogenesis, and ultimately potential applications in bone tissue engineering. To achieve these, six sol-gel copper/magnesium substituted derivatives of 58S-BG, i.e. a mol% series of $60SiO_2$-$4P_2O_5$-5CuO-(31-x) CaO/xMgO (where x=0, 1, 3, 5, 8, and 10), were synthesized. Afterwards, the effect of MgO/CaO substitution on the *in vitro* formation of nano-hydroxyapatite (HA), osteoblast-like cell responses and BGs antibacterial performance were studied. During the BGs synthesis, the elimination of nitrates was achieved at 700 °C that prevented the BGs crystallization and stabilized the obtained dried gels. The structural and morphological evaluations were performed with X-ray diffraction (XRD), Fourier transform infrared spectroscopy (FTIR), and scanning electron microscopy (SEM). These characterizations revealed that Cu-substituted 58S-BG consisting of 5 mol% MgO (BG-5/5) slightly had retarded the formation of HA. In addition, Cu-substituted 58S-BGs consisting 8 mol% and 10 mol% MgO (BG-5/8 and BG-5/10) displayed lower bioactivity probably due to the lower ion release rate of Ca–Si into the simulated body fluid (SBF). The determination of 3-(4, 5 dimethylthiazol-2-yl)-2, 5-diphenyltetrazolium bromide (MTT) and alkaline phosphate (ALP) activities proved that the highest values of both differentiation and proliferation of MC3T3-E1 cells can be obtained from a 5 mol% MgO substituted BG, while the over addition of MgO (8 mol% and 10 mol%) decreased the bioactivity. Furthermore, these novel Cu/Mg-substituted 58S-BGs displayed antibacterial effect against methicillin-resistant *Staphylococcus aureus* bacteria. Taken together, the results suggest the equally-substituted BG-5/5 (i.e. the one consists of 5 mol% of both CuO and MgO) as a promising candidate for bone tissue engineering, among all newly designed BGs in this work, owing to its desirable cell proliferation, ALP activity and antibacterial properties.

***Keywords*—**Apatite, bioactivity, biomedical applications sol-gel processes.

I. Introduction

BONE tissue engineering aims for the regeneration and replacement of skeletal tissues damaged through trauma, osteoporosis, and aging-related degenerative diseases [1]-[3]. This technology has introduced numerous biomaterials suitable for bones repair and replacement [4]. Among these materials, a subset of amorphous silicate composites, namely BGs, has played a significant role in establishing a platform of bone repair [5], [6]. BGs are commonly synthesized by sol-gel technique as a reliable substitute for traditional melt quenching method. The sol-gel process is performed at room temperature and prevents the evaporation of volatile starting materials like P_2O_5, and hence results in a higher purity and homogeneity of the products [7]–[9]. In addition, the sol-gel method provides a facile and uniform incorporation of various inorganic ions into the BGs structure.

The incorporation of elemental additives such as alkali [10], alkaline earth [11]–[13], transition [14], [15] and post-transition [16], [17] metals enhances BGs performance and introduces osteoconductivity [17], [18], angiogenicity [15], [19] and antibacterial properties [15], [20]. Magnesium (Mg) is the fourth most abundant metal cation in the human body and the second most common intracellular cation [21] and approximately 50–60% of Mg total content is stored in the skeleton [22]. Magnesium deficiency is found to be a possible risk factor of osteoporosis [23] and the relevant literature has revealed that magnesium deficient diets lead to the inhibition of bone growth [24]–[26]. Therefore, Mg plays an important role in bone formation, osteoblast cell activity enhancement, and osteoclasts inhibition. On the other hand, copper is an essential trace metal existing in living organisms and is necessary for triggering some of the biological processes. Copper is known as an angiogenic reagent due to its role in the increase of pro-angiogenic expression and stimulation of the human endothelial cell proliferation [27]–[29]. Previous reports have suggested that the incorporation of 5 mol% CuO in BG composition can result in a significant antibacterial efficiency [15], and an improved bone regeneration capability and a higher angiogenesis stimulation compared to copper-free BGs. For example, Wu et al. [15] obtained a significant AlP activity and stimulated vascular endothelial growth factor (VEGF) expression in human bone marrow stromal cells (hBMSCs) from BGs containing 5 mol% CuO. In addition, Li et al. [30] introduced a few Cu-BG coated nanocomposites (5 mol% CuO) on the natural eggshell membrane that stimulated angiogenesis and proangiogenesis by improving VEGF during the wound healing process. Furthermore, Ye et al. [31] designed a CuO substituted mesoporous BG (SiO_2-CaO-P_2O_5-SrO, 5 mol% Cu-MBG) suitable for coating applications. The latter modified the porous HA structures and acquired a potent antibacterial activity against *E. coli* and *S. aureus* bacteria. Having all these in mind, a fixed amount of CuO (5 mol%) was allocated as the optimal copper content in the synthesis of

Moghan Amirhosseinian and Amir Khaleghipour are with the Department of Materials Engineering, Imam Khomeini International University, Qazvin, 34149-16818, Iran.

Elhamalsadat Ghaffari is with the Department of Materials Engineering, Imam Khomeini International University, Qazvin, 34149-16818, Iran (corresponding author, phone: +98 9120725192, fax: +09833901186, e-mail: moghanian@aut.ac.ir).

Cu/Mg-substituted 58S-BGs in this work.

Although several studies on Mg-substituted BGs are found within the literature, no effect of Mg content on the formation of HA layer and its *in vitro* bioactivity have been precisely elucidated to date. Some of these investigations indicated that a delay in the formation of HA occurs in the presence of Mg ions [32]–[35]. Controversially, the examples of Mg's improving effect on BGs bioactivity [36]–[39], as well as its insignificant role in the formation of HA are also found in the literature [40]. For instance, Erol et al. [39] demonstrated that MgO in the CaO-SiO_2-P_2O_5-MgO BGs can increase the rate of HA layer formation. Moreover, some MgO-substituted BGs (10 mol%) in Prabhu's research [38] displayed a higher bioactivity in comparison with MgO-free BGs. However, Salinas et al. [41] believed that the increase of MgO content in SiO_2-CaO-MgO may not necessarily affect *in vitro* bioactivity of BGs. In agreement with the common perception, Ma's group [33] found that substituting MgO (0–20 mol%) for CaO, in sol-gel derived BGs, retards the HA layer formation.

An optimal substitution ratio of MgO/CaO in BG composition that may significantly improve the cell proliferation and activity is yet to be discovered. In 2009, a sol-gel derived SiO_2-CaO-P_2O_5-MgO BG consisting 5 mol% CaO/MgO showed an increase of the differentiation of human fetal osteoblastic cells (hFOB 1.19) in Saboori's work [42]. Later on, Wang et al. [43] reported that SiO_2-CaO-P_2O_5 BGs doped with 2.25 mol.% MgO demonstrate a higher proliferation and ALP activity of mesenchymal stem cells (MSCs). However, Balamurugan et al. [44] had already claimed that sol-gel derived SiO_2-CaO-MgO-P_2O_5 BG with 13 mol% MgO enhances the proliferation and activity of human osteoblast-like cells (MG63). Finally, Prabhu et al. [38] in 2013 suggested that the substitution of 10 mol% of CaO by MgO in $58SiO_2$–$33CaO$–$9P_2O_5$ (mol%) BG has a stimulating effect on the human gastric adenocarcinoma (AGS) cells proliferation and activity.

Infections around implanted biomaterials may occur for various reasons and always make surgeons concerned [45]. Bacterial infections may delay wound healing processes and even lead to surgical failures [46]. The implantation of these materials requires additional protection mechanisms to prevent every bacteria growth [47]. Therefore, implant biomaterials designed for specific clinical application must be as anti-infective as required [48].

As mentioned above, both Mg- and Cu-substituted BGs have stimulatory effects on osteogenesis, angiogenesis and often show anti-bacterial activities. These two have been separately utilized as BGs dopants. To the best of our knowledge, until now, no comprehensive study has reported on the synthesis and *in vitro* application of Cu/Mg substituted 58S bioactive glasses (CM-BG). Therefore, this study elaborates on the effect of MgO substituting for CaO on the bioactivity, biocompatibility, Alp activity and antibacterial efficiency of the sol-gel derived Cu/Mg-substituted 58S BGs and suggests an optimal percentage of MgO in 58S-BG to achieve the highest cell proliferation and activity as well as antibacterial activity against MRSA bacteria. To achieve these goals, here we synthesize a series of sol-gel derived 58S-BGs consisting MgO (with a concentration range of 0 to 10 mol%) accompanied with a fixed concentration CuO (5 mol%). In addition, the effect of Mg on MC-BGs *in vitro* reactivity is studied by the samples immersion in a SBF and observing the morphological change of CM-BGs upon the formation of hydroxycarbonate apatite (HCA) on their surfaces. The *in vitro* formation of HCA is monitored by ICP-AES, FTIR, XRD, and SEM. Moreover, MTT and ALP activity assays are performed to complement the *in vitro* biological investigations. Furthermore, the bactericidal efficiency of CM-BGs is evaluated against MRSA bacteria.

II. Materials and Method

A. Materials

Tetraethyl orthosilicate (TEOS), triethyl phosphate (TEP), calcium nitrate tetrahydrate $Ca(NO_3)_2.4H_2O$, copper(II) nitrate trihydrate and magnesium nitrate hexahydrate were used in the synthesis of Cu/Mg-substituted 58S BGs as the sources of SiO_2, CaO, P_2O_5, MgO and CuO in BGs composition. Also, NaCl, KCl, $K_2HPO_4.3H_2O$, $MgCl_2.6H_2O$, $CaCl_2$, Na_2SO_4, tris(hydroxymethyl) aminomethane $(HOCH_2)_3CNH_2$, and HCl were used in the preparation of SBF as described in the literature [49]. All the chemicals are purchased from Merck (Darmstadt, Germany) and directly used without any further purification. The MC3T3-E1 mouse osteoblast-like cell lines used in our biological investigations were supplied by Sigma-Aldrich (Poole, UK). The standard cell culturing was performed in glutamine (2 mM) supplemented α-MEM consisting antibiotic additives (1%), fetal bovine serum (10%, Sigma-Aldrich, UK), and penicillin-streptomycin (0.1%) under a humidified atmosphere of CO_2–air 5% kept at 37 °C. The culture medium was refreshed by a total replacement once for any given 2-day period. The confluent cells were detached with trypsin and sub-cultured into three passages which were later used for the *in vitro* biological experiments.

B. BG Synthesis

Six copper-substituted 58S-BGs of the series $60SiO_2$-$4P_2O_5$-5 CuO-(31-x) CaO- xMgO, (x=0; 1; 3; 5; 8 and 10 on molar basis) were synthesized through the sol-gel method as follows. First, distilled water, 0.1 M nitric acid and TEOS, were mixed by a magnetic stirring bar for 1 h at room temperature. Then, TEP, $Ca(NO_3)_2{\cdot}4H_2O$, Cu $(NO_3)_2.3H_2O$ and $Mg(NO_3)_2.6H_2O$ were respectively added with 45 min intervals for each reagent to get fully homogenized. The final mixture was stirred for one more hour to assure that the hydrolysis is accomplished. The prepared solution (sol) was poured into a teflon container and kept sealed at 37 °C for 3 days and then dried over 24 h at 75 °C. Finally, the dried gel was then calcined over 3 h in a furnace at 700 °C to eliminate the nitrate and other organic residues. The obtained calcined powders were transferred into a zirconia planetary ball mill (Retsch, Germany) and ground into a fine powder (final particle size < 50 μm). Afterwards, the retrieved fine powder was reshaped into tablets (Ø10×3 mm) under the pressure of

(9 MPa) a manual hydraulic press. The detailed compositions of the produced CM-BGs are presented in Table I.

TABLE I
ELEMENTAL COMPOSITIONS OF THE CU/MG-SUBSTITUTED 58S-BGS (IN MOL %)

Glass	Label	SiO_2	CaO	P_2O_5	CuO	MgO
58S- 0%CuO-0%MgO	BG-0	60	31	4	5	0
58S- 5%CuO-1% MgO	BG-5/1	60	30	4	5	1
58S- 5%CuO-3% MgO	BG-5/3	60	28	4	5	3
58S- 5%CuO-5% MgO	BG-5/5	60	26	4	5	5
58S- 5%CuO-8% MgO	BG-5/8	60	23	4	5	8
58S- 5%CuO-10% MgO	BG-5/10	60	21	4	5	10

C. Preparation of SBF

The SBF solution was prepared by the Kokubo's procedure [49] as follows. Reagent-grade sodium chloride (NaCl), potassium chloride (KCl), sodium bicarbonate ($NaHCO_3$), sodium sulfate (Na_2SO_4), magnesium chloride hexahydrate ($MgCl_2.6H_2O$), calcium chloride ($CaCl_2$), di-potassium hydrogen phosphate trihydrate ($K_2HPO_4{\cdot}3H_2O$) and tris(hydroxymethyl)aminomethane (TRIS) dissolved in distilled water. The pH of the obtained solution was adjusted at 7.25 by the addition of hydrochloric acid (HCl, 1N) at 37 °C. The composition of the SBF solution was compared with the human blood plasma (Table II).

TABLE II
COMPOSITION OF SBF SOLUTION AND HUMAN BLOOD PLASMA (MMOL.L–1)

Ion	Plasma (mmol.L^{-1})	SBF (mmol.L^{-1})
Na^+	142.0	142.0
K^+	5.0	5.0
Mg^{+2}	1.5	1.5
Ca^{+2}	2.5	2.5
Cl^-	103.0	147.8
HCO_3^{-1}	27	4.2
HPO_4^{-2}	1.0	1.0
SO_4^{-2}	0.5	0.5

D. Characterization of BGs

1. Thermal Analysis

The differential thermal (DTA) and thermogravimetric (TGA) analyses of BG-5/0 and BG-5/10 were performed to determine the suitable sintering temperature for dried gels. The TGA and DTA thermograms were recorded by a Shimadzu TGA-50 that heated the BGs (25–1100 ±5 °C, 10 ± 0.5 °C.min^{-1}) under the constant flow of an inert gas (N_2, 60 mL.min^{-1}).

2. XRD

The compositional changes of the BG phase, before and after soaking the BGs in SBF, were monitored by XRD (INEL-Equinox-3000, France). The surface of BG-5/5, the selected BG owing to the MTT, ALP and cell proliferation results, were analyzed with a Cu Kα X-ray (λ =1.5405 A°) at 40 kV in the $20° \leq 2\theta \leq 50°$ interval.

3. FTIR

HA phase formation on the surface of BG-5/5 was determined by FTIR (Nicolet Avatar 660, Nicolet) spectrum. Scarped material from BG-5/5 surface (1 mg) was mixed with KBr (spectroscopy grade, 100 mg), palletized under vacuum and scanned with a resolution of 8 cm^{-1} in the wavenumber range of 400–4000 cm^{-1}.

4. Inductively Coupled Plasma-Atomic Emission Spectroscopy (ICP-AES)

The concentrations of Ca, Si, P, Cu and Mg ions in SBF solution were measured by ICP-AES (Varian Vista Pro, Palo Alto, USA). During the *in vitro* experiments, the disk-shaped BGs were immersed in SBF solution and incubated at 37 °C for 1, 3, 7 and 14 days. The ratio of CM-BGs surface area to the applied SBF volume was kept constant (approx. 0.1 $cm^2.mL^{-1}$). At the selected immersion time periods, the disk-shaped CM-BGs were removed from the SBF, gently rinsed with distilled water and dried at room temperature. All the aforementioned ions were traced within the reacted SBF solutions, and their concentrations were compared with the original values.

5. pH Measurement

A calibrated pH meter (Corning 340, USA) monitored the pH value of the SBF solution during the BGs immersion as displayed in Fig. 5.

6. SEM

The morphological evolution of BG-5/5 surface was observed by SEM (Philips XL30, Netherland). The effect of Mg on the morphology of the nano-sized HA, formed after the immersion of BG-5/5 in the SBF, was also investigated. The BG sample was coated with a thin layer of gold (Au) by sputtering (EMITECH K450X, England).

E. Biological Evaluation

1. MTT Assay

MTT assay was performed to evaluate the cell viability and proliferation of MC3T3-E1 cells seeded on the surface of the CM-BGs for 1, 3 and 7 days. First, cells were seeded on CM-BGs into a 96-well plate at a density of 6×10^3 cells per well with regular DMEM medium and incubated for the mentioned periods. At the end of incubation periods (days 1, 3 and 7), the medium was removed and 100 µL of a 5 mg.mL^{-1} solution of MTT (Sigma Aldrich) in phosphate buffered saline (PBS) was added to the culture medium. After 4 h of incubation at 37 °C, the culture medium was pipetted out and dimethyl sulfoxide

(DMSO, Sigma) was applied for dissolving the formazan crystals. Finally, a multi-well microplate reader (EL 312e Biokinetics reader, Biotek Instruments) recorded the solutions optical density (OD) at a wavelength of 570 nm and cells cultured in the absence of CM-BGs were used as the control.

2. Alkaline Phosphatase (ALP) Activity

The ALP activity, one of the phenotypic markers for osteoblast proliferation and differentiation, was evaluated based on the method that Lawry et al. described [50] using *p*-nitrophenyl phosphate. Accordingly, the cellular ALP was determined by monitoring the conversion of *p*-nitrophenyl phosphate to *p*-nitrophenol [51]. The enzyme activity was evaluated for each specimen by the recorded absorbance at 410 nm and the amount of liberated *p*-nitrophenol [52]. The procedure was performed in accordance with the manufacturer's guidelines (BioCat, Heidelberg, Germany). First, cells were counted and plated in 24-well plates at a density of 1×10^4 cells.cm^{-2} and cultured with CM-BGs in a humidified atmosphere of CO_2–air (5%) at 37 °C. After 1, 3 and 7 days, the supernatant fluid was carefully removed and the cell layer was gently rinsed with PBS. Afterward, Tris buffer (1mL) was added and sonicated (4 min on ice) until become homogenized. A series of 20 µl aliquots were mixed in *p*-nitrophenyl phosphate solution (1 mL, 16 mmol.L^{-1}, Sigma) and stored at 30 °C for 5 min. Also, the blanks were similarly prepared as described above.

3. Antibacterial Studies

The effect of the coexistence of Cu and Mg on the BGs antibacterial activity, against MRSA bacteria, was investigated with a previously described method [53]. First, cultured MRSA in liquid lysogenybroth (LB) medium was diluted to reach to approx. $0.5 – 2 \times 10^8$ mL^{-1} [53]. Then, LB medium (0.9 mL) was transferred into sterile tubes (1.5 mL Eppendorf) containing CM-BG particles (10 mg) and shaken for 1 min. Afterwards, bacterial suspension (0.1 mL) was injected into the Eppendorf tubes and then incubated (37 °C, 1 h). Once serial dilutions were performed, these suspensions (100 µL) were transferred onto LB-agar plates and stored in dark (37 °C) over-night [53]. The resultant colonies were counted as colony-forming units per milliliter (CFU/mL), and the bactericidal percentages were calculated according to the literature [53], [54] as follows.

Bactericidal fraction = 1– (number of survived bacteria / total number of bacteria)

F. Statistical Analysis

GraphPad Prism software package (V. 3.0, GraphPad Prism, USA) performed the statistical analysis. The cell assays and elemental analysis were collected from three samples of each group. Quantitative data were expressed as means ± standard deviations (SD) and the corresponding p-value significance was only considered at *p<0.05. (*p < 0.05, **p < 0.01 and ***p < 0.001).

III. Results and Discussion

A. Thermal Analysis

The DTA and TGA thermograms of two BG samples are shown in Figs. 1 (a) and (b), respectively. The first endothermic DTA peaks appeared at around 140 °C indicated the dehydration of the BG samples, while the condensation of silanols and the elimination of nitrates occurred between 220 and 600 °C [18], [42], [55]. Once the nitrates were completely removed (above 600 °C), the TGA thermograms leveled between 43–48% and displayed no more changes. The exothermic crystallization peaks of BG-5/0 and BG-5/10 appeared at around 950 and 900 °C, respectively. The crystallization temperature of BG-5/10 found to be lower than BG-5/0 owing to its lower viscosity and faster element diffusion caused by MgO presence. According to the results of DTA/TGA analyses, 700 °C was found as a suitable temperature for the stabilization of CM-BGs.

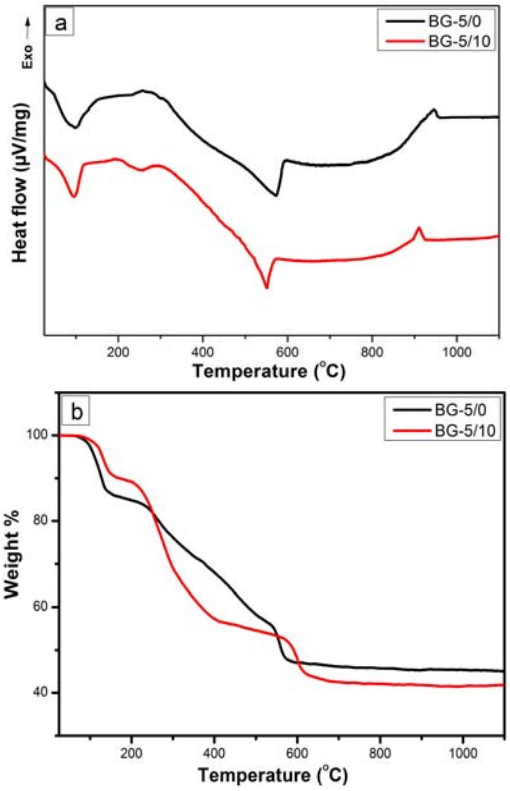

Fig. 1 DTA (a) and TGA (b) thermograms of BG-5/0 and BG-5/10 (30 – 1100 °C ± 5 °C)

B. Phase Analysis

The XRD patterns of BG-5/5, at different soaking periods in SBF solution, are presented in Fig. 2. The glassy characteristics and amorphous structure of BG-5/5 were confirmed by the XRD prior the immersion. After the immersion, on days 1 and 3, the surface of BG-5/5 seemed amorphous and its glassy nature was confirmed by finding no XRD peaks. According to a standard (HA; JCPDS 09-432), the characteristic diffraction peaks at 2θ: 25.8° and 31.8° are assigned for (200) and (211) atomic planes in HA lattice,

respectively [56]. After 7 days of immersion, an emerging peak at 31.8° (2θ) was detected (Fig. 2) and 7 days later another peak was found at 25.8° (2θ). A gradual increase in peak intensity of (211) plane was also observed from 7th to 14th day. Accordingly, XRD results proved that BG-5/5 was capable of *in vitro* HA formation.

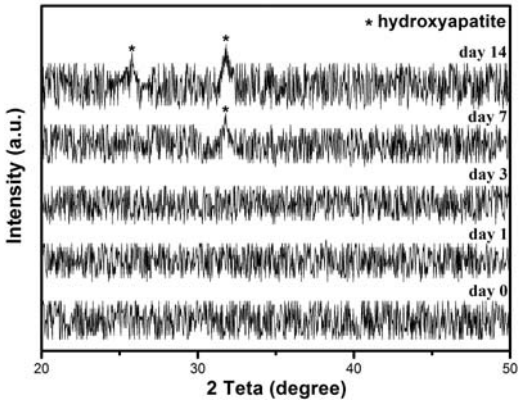

Fig. 2 The XRD patterns of BG-5/5 before and after 1, 3, 7 and 14 days of soaking in SBF

C. Structural Groups

Fig. 3 presents the FTIR spectra of BG-5/5 before and after being immersed in SBF solution at various time periods. Prior to the immersion, BG-5/5 only showed the finger prints of silicate network on its FTIR spectra due to the presence of SiO_2 as its major component. In Fig. 3, the main infrared bands appear at 470, 790, 922, 1066 and 1250 cm^{-1} indicating the silicate network and respectively are assigned to the bending of Si–O–Si, symmetric stretching of Si–O bridging oxygen atoms between the tetrahedrons, stretching of Si–O nonbridging oxygen atoms, symmetric and asymmetric Si–O–Si stretching [57]. Moreover, the infrared bands of PO_4^{3-} (609 cm^{-1} [58]) and hydroxyl group (3500 and 1651 cm^{-1}) are shown in Fig. 3.

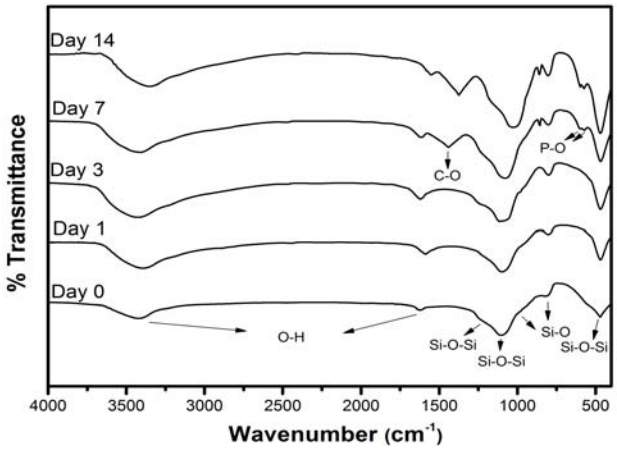

Fig. 3 FTIR spectra of BG-5/5 before and after various soaking periods

The elongated immersion of BG-5/5 resulted in a few new FTIR peaks which confirmed the formation of HA on its surface [59]. After 7 days of immersion in SBF solution, two additional FTIR peaks, at around 1455 and 870 cm^{-1}, were detected which stand for carbonates C–O stretching substituted for the phosphates in HA lattice. Moreover, the P–O absorption bands emerged as two resolved peaks with increasing intensity at 570 and 600 cm^{-1} which are expected for crystalline HA [60]. Therefore, the FTIR spectra supported the XRD patterns by revealing the crystalline nature of the newly formed material on the surfaces of BG-5/5. These indicated the expected figure prints and XRD peaks of bone-like HA (at 2θ= 25.8° and 31.8°) at the 7th day of immersion and the peak intensities increased by increasing the immersion time due to the maturation of HA on the surface. These confirmed the *in vitro* HA formation ability of BG-5/5.

D. Ion chemistry of SBF solution

Figs. 4 (a)-(e) indicates the variations of Ca, Si, P, Cu and Mg concentrations in the SBF solution for different soaking periods in SBF solution. Accordingly, during the first 3 days of immersion, Ca concentrations of BG-5/0, BG-5/1, BG-5/3, BG-5/8 and BG-5/10 rapidly increased from 100 mg/L to 305.9, 299.7, 290.1, 279.3, 287.4 and 279.6 mg/L, respectively. These values gradually decreased during the following days and reached to 191.3, 188.1, 185.3 and 180.7 mg/L respectively for BG-5/0, BG-5/1, BG-5/3 and BG-5/5 on the 7th day of the immersion; While, BG-5/8 and BG-5/10 showed a different trend and respectively reached to 154.4 and 159.8 mg/L. According to a previously suggested mechanism [61], these Ca concentration trends reveal the occurrence of Ca ions dissolution from BGs to SBF solution and then precipitation of the Ca ions from SBF solution on the BGs surface during the crystallization of HA. This postulation was confirmed by both XRD and FTIR results which showed no HA peaks after the first day of immersion for BG-5/5 and also no changes were observed in XRD and FTIR results for longer time up to the 7th day. Furthermore, at this point of the test the CM-BGs with high Mg contents, like BG-5/8 and BG-5/10, showed higher values of Ca concentration than other synthesized CM-BGs which had lower Mg content, e.g. BG-5/5 (Fig. 4 (a)). Fig. 4 (b) shows the poor solubility of Si which is even more decreased by the presence of Mg; for example, BG-5/10 displayed the lowest concentration of Si. In fact, Mg^{2+} ion has a smaller ionic radius, 72 pm compared to 99 pm for Ca^{2+}, and higher field strength which compacts the BGs structure. This prevents an easy penetration of SBF solution inside the CM-BGs structures and hence Si ion exchange is interrupted. According to Figs. 4 (a) and (b), the quick release of Ca and Si ions from CM-BGs and the subsequent HA formation can be considered as the main factors in the rapid bonding of BGs to bone tissues [62]. The changes of P concentration over soaking time (Fig. 4 (c)) did suggest that an increase of Mg content in BGs could decrease the HA precipitation rate. Fig. 4 (d) showed that increasing the Mg content, from 1 to 10 mol% in Cu-substituted 58S-BG, relatively slowed the release of Cu ions. This slowed ion release can be taken as another sign for the tightly packed networks due to the higher field strength of Mg^{2+} ions

compared to Ca^{2+}. Therefore, Figs. 4 (d) and (e) demonstrated that during the early soaking stages the concentrations of Cu^{2+} and Mg^{2+} were increased until about the 3rd day and after that reached a plateau on day 7th and remained the same afterwards. This decreased dissolution rate of Cu^{2+} and Mg^{2+} ions might be due to the formation of silica rich and HA-covered layers on the surfaces of CM-BGs.

E. pH Measurement

The pH values of the SBF solutions are displayed in Fig. 5. The Ca^{2+}, Mg^{2+}, Cu^{2+} and H^{+} ions exchange accompanied by the SBF solution proton depletion as well as a gradual increase in Mg^{2+}concentration. These phenomena led to a pH increase during the immersion time. This increase of pH progressively slowed down due to the decreasing Ca^{2+} concentrations caused by HA formation [57]. In addition, the pH values of CM-BGs with high Mg content such as BG-5/8 and BG-5/10 were found to be higher than other CM-BGs with less Mg content such as BG-5/1, BG-5/3 and BG-5/5 (Fig. 5).

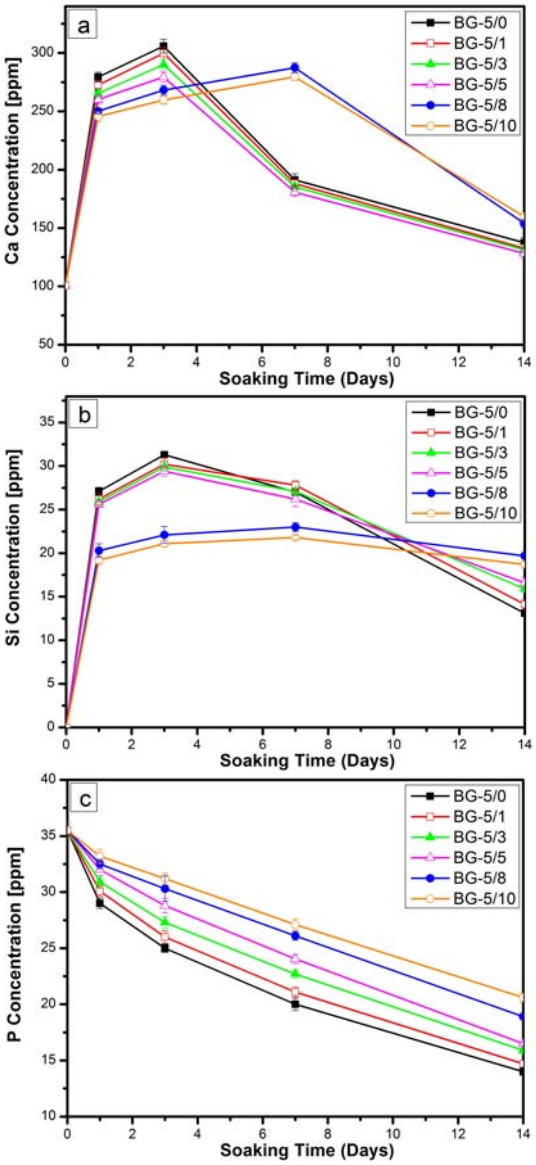

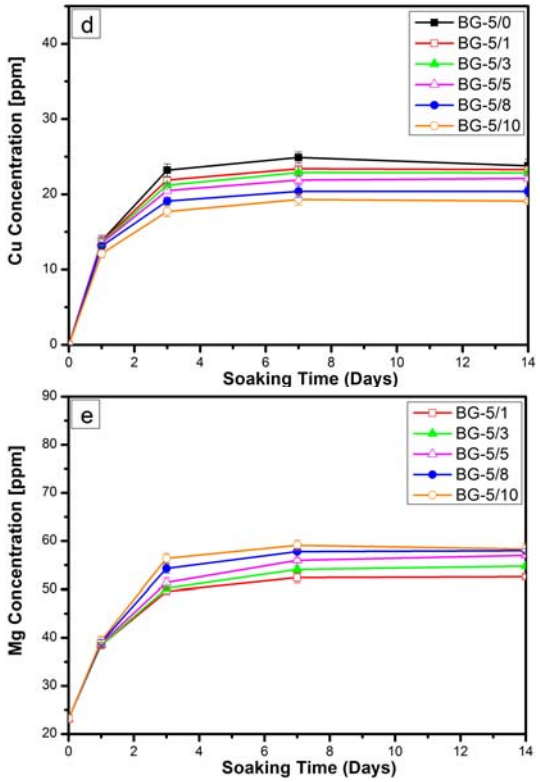

Fig. 4 Calcium (a), silicon (b), phosphorus (c), copper (d) and magnesium (e) ions concentrations in the SBF solution monitored during the soak

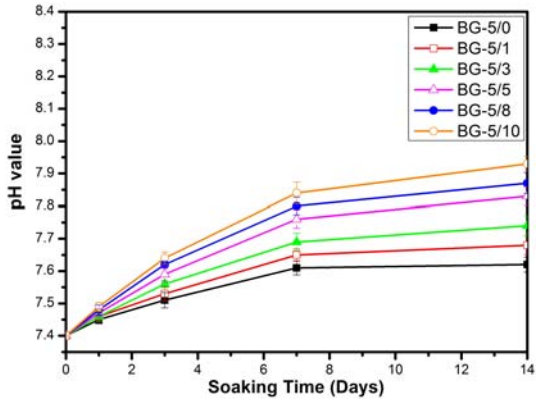

Fig. 5 The SBF pH variation versus soaking time of the synthesized CM-BGs

F. Surface Microstructures

Various properties of the BGs can be assessed by investigating the changes in the morphology of surfaces [12]. Figs. 6 (a)–(e) displays the SEM micrographs of BG-5/5 before and after soaking in SBF solution. Before soaking in the SBF (Fig. 6 (a)), the SEM revealed that no HA particles existed and no significant morphological changes were observed during the following two days except some regional HA nucleation site were found. On 7th day of soaking, the surface of BG-5/5 was partially covered by the *in-situ* formed HA that was simply observed by SEM (Fig. 6 (d)). The HA layer matured over the following days and SEM showed (Fig.

6 (e)) that the surface of BG-5/5 was completely covered by nano-size HA. A high-magnified SEM image (Fig. 6 (f)) showed nano-size worm-like HA particles formed on BG-5/5 surface during 14 days of immersion in SBF. A similar worm-looking morphology of HA is previously reported by Chen et al. [63] that was formed on the surface of MgO–CaO–SiO_2 bioglass. According to the SEM observations, HA formation on BG-5/5 surface during its immersion in SBF solution was in agreement with FTIR and XRD results.

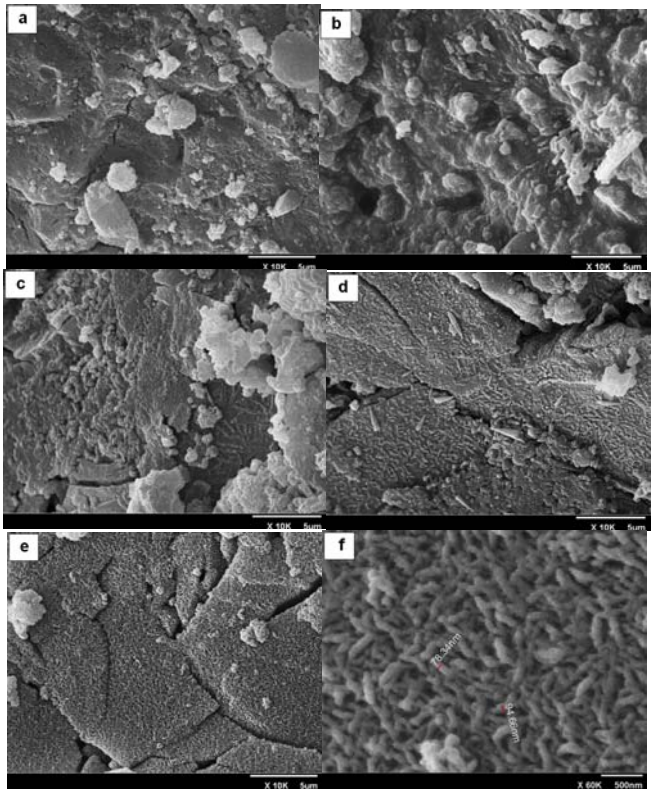

Fig. 6 SEM images of BG-5/5 before (a) and after soaking in the SBF solution for 1 (b), 3 (c), 7 (d) and 14 (e) days at magnification 10K×; and image (e) at 60K× magnification (f)

J. In vitro Biological Evaluation

1. Cell Proliferation

The proliferation of the osteoblast-like cell line, MC3T3-E1, cultured on various CM-BGs for 1, 3 and 7 days are shown in Fig. 7. On the first day of culturing, BG-5/5 sample showed a statistically significant increase ($^{*}p<0.05$) in comparison with the control and BG-5/0, while no significant differences were observed in the MTT activities of cells incubated with other CM-BGs compared to the control ($^{*}p>0.05$). After 3 days in culture, MTT activity was significantly higher in the cells in presence of dissolution ions from BG-5/3 and BG-5/5 compared to the control ($^{**}p<0.01$). Meanwhile, the cells in presence of BG-5/3 and BG-5/5 exhibited same proliferation (no statistically significant difference: $^{*}p >0.05$). Additionally, MTT values increased over the time and reached to the maximum after 7 days. Previously, Saboori et al. [42] reported that the presence of 5 mol% Mg in 64% SiO_2-26% CaO-5% MgO-5% P_2O_5 (based on mol%) BG resulted in a significant increase in proliferation of human fetal osteoblastic cells (hFOB 1.19). Based on the results of the MTT assay, the simultaneous presence of 5 mol% of Cu and Mg in the 58S-BG composition (BG-5/5) led to a more statistically significant increase in MC3T3-E1 cells proliferation compared with BG-5/0 ($^{**}p< 0.01$).

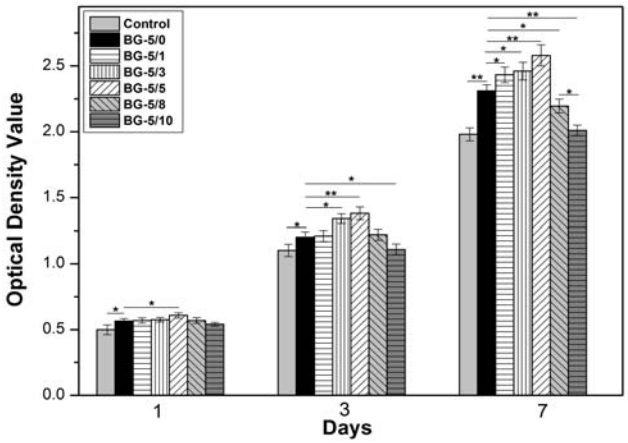

Fig. 7 Osteoblast-like cell line proliferation (MC3T3-E1), cultured on the synthesized CM-BGs for 1, 3 and 7 days. ($^{*}p < 0.05$ and $^{**}p < 0.01$)

2. Cell Activity

The ALP activity of the osteoblast-like cell line (MC3T3-E1) cultured on CM-BGs for 1, 3 and 7 days is displayed in Fig. 8. As observed, the ALP activity constantly grew up to the 7th day. Furthermore, the ALP activities of cells in contact with CM-BGs reached their maximum on day 7 which were approximately 4 times greater than the first day. Each culturing batch showed statistically significant differences which were measured by the ALP activity of cells treated with BG-5/5 with respect to the BG-5/0 ($^{*}p< 0.05$). Interestingly, BG-5/5 showed the highest ALP activity in each culturing time and the decrease of ALP activity by the increasing Mg content, from 5 to 10 (in mol%), was in a good agreement with MTT results. Moreover, the substitution of 10 mol% MgO for CaO in BG-5/10, significantly decreased the ALP activity of MC3T3-E1 cells in comparison with BG-5/0 ($^{*}p< 0.05$).

3. Antibacterial Studies

As shown in Fig. 9, the simultaneous presence of Cu and Mg in 58S-BGs led to a significant antibacterial effect against MRSA bacteria. The samples contained 3 mol% and 5 mol% MgO (BG-5/3 and BG-5/5), in bacterial suspension (with fixed concentration of 10 mg/mL), demonstrated the maximum bactericidal percentage to MRSA bacteria with no statistically significant difference ($^{*}p>0.05$). Also, antibacterial activity decreased by increasing the Mg content in CM-BGs compositions (BG-5/8 and BG-5/10). The exact mechanism of BGs antibacterial activities is not discovered yet [64]; however, some factors are possibly involved like the presence of ions such ad calcium [64], phosphate [64], copper

[30], [31], [65] and magnesium [66] as well as the pH value proposed due to the release of alkali ions [53], [67]. According to the antibacterial study, BG-5/3 and BG-5/5 showed the most efficient antibacterial effects against MRSA bacteria with respect to the rest of the synthesized CM-BGs in this work.

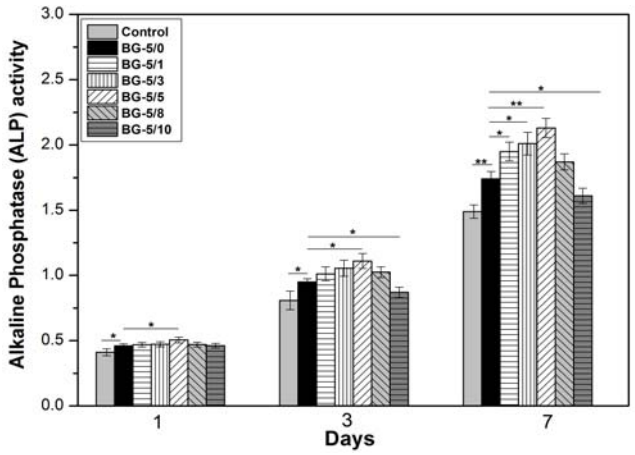

Fig. 8 ALP activities of osteoblast-like cell line (MC3T3-E1) cultured on synthesized CM-BGs for 1, 3 and 7 days. (*p < 0.05 and **p < 0.01)

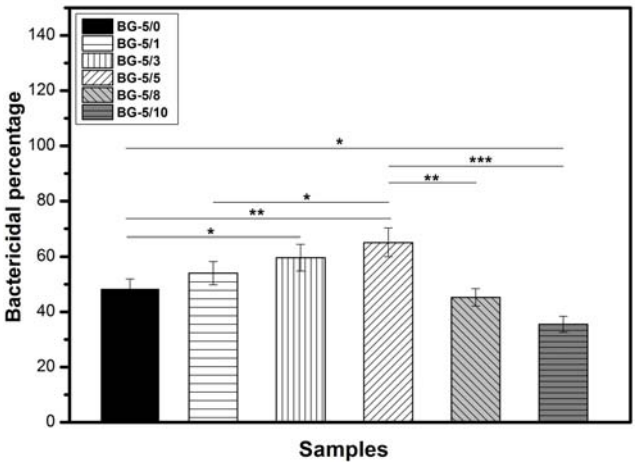

Fig. 9 The bactericidal percentages of 10 mg/mL of BG-5/0 (control), BG-5/1, BG-5/3, BG-5/5, BG-5/8 and BG-5/10. (*p < 0.05, **p < 0.01 and ***p < 0.001)

IV. Conclusions

In summary, six 58S-BGs incorporated with a fixed concentration of Cu (5 mol%) and the variable Mg concentrations (in range of 0, to 10 mol%), in $60SiO_2$-$4P_2O_5$-5CuO-(31-x)CaO- xMgO, (x=0; 1; 3; 5; 8 and 10 on molar basis) system, were successfully synthesized through the sol-gel method and the synergetic effect of Cu and Mg on 58S-BG was investigated. The reveal of C–O stretching and P–O absorption bands in FTIR spectra and the detection of characteristic peaks of crystalline HA as well as monitoring the surface morphology evolution, confirmed the formation of a nano-size crystalline HA on the surface of the 58S-BG incorporated with 5 mol% CuO and 5 mol% MgO (BG/5-5) after soaking in SBF solution. In addition, *In vitro* studies with MC3T3-E1 cells showed that BG-5/5 was non cytotoxicalso based on biological results and BG-5/5 significantly increased cell proliferation and alkaline phosphatase activity of MC3T3-E1 cells. Furthermore, BG-5/5 exhibited the highest bactericidal efficiency against MRSA bacteria among all newly designed Cu/Mg-substituted 58S-BGs in this work. Therefore, BG-5/5 is introduced as a novel candidate with multi-functional properties desired for bone tissue engineering. Further investigations will be carried out to clarify how exactly the presence of Cu and Mg in BGs does increase the MTT, ALP and antibacterial activity. We also aim for developing the clinical use of this novel biomaterial and employ it in the design of light-triggered [68] and targeted drug delivery [69] systems in the forthcoming future.

References

[1] K. H. Karlsson, L. Hupa, Thirty-five years of guided tissue engineering, J. Non. Cryst. Solids. 354 (2008) 717–721.
[2] G. Dickson, F. Buchanan, D. Marsh, E. Harkin-Jones, U. Little, M. McCaigue, Orthopaedic tissue engineering and bone regeneration, Technol. Heal. Care. 15 (2007) 57–67.
[3] B. Sharma, S. Varghese, Progress in orthopedic biomaterials and drug delivery, Drug Deliv. Transl. Res. 6 (2016) 75–76.
[4] T. Kokubo, Nihon Medikaru Materiaru Kabushiki Kaisha., Bioceramics and their clinical applications, Woodhead Pub. and Maney Pub. on behalf of Institute of Materials, Minerals & Mining, 2008.
[5] M. Laczka, K. Cholewa-Kowalska, A. M. Osyczka, Bioactivity and osteoinductivity of glasses and glassceramics and their material determinants, Ceram. Int. 42 (2016) 14313–14325.
[6] L. L. Hench, The story of Bioglass®, J. Mater. Sci. Mater. Med. 17 (2006) 967–978.
[7] P. Sepulveda, J. R. Jones, L. L. Hench, Characterization of melt-derived 45S5 and sol-gel-derived 58S bioactive glasses, J. Biomed. Mater. Res. 58 (2001) 734–740.
[8] D. Arcos, D. C. Greenspan, M. Vallet-Regí, A new quantitative method to evaluate the *in vitro* bioactivity of melt and sol-gel-derived silicate glasses, J. Biomed. Mater. Res. Part A. 65A (2003) 344–351.
[9] R. Ravarian, F. Moztarzadeh, M. S. Hashjin, S. M. Rabiee, P. Khoshakhlagh, M. Tahriri, Synthesis, characterization and bioactivity investigation of bioglass/hydroxyapatite composite, Ceram. Int. 36 (2010) 291–297.
[10] A. Moghanian, S. Firoozi, M. Tahriri, Synthesis and in vitro studies of sol-gel derived lithium substituted 58S bioactive glass, Ceram. Int. 43 (2017) 12835–12843.
[11] A. Moghanian, S. Firoozi, M. Tahriri, Characterization, in vitro bioactivity and biological studies of sol-gel synthesized SrO substituted 58S bioactive glass, Ceram. Int. 43 (2017).
[12] J. Ma, C. Z. Chen, D. G. Wang, X. Shao, C. Z. Wang, H. M. Zhang, Effect of MgO addition on the crystallization and in vitro bioactivity of glass ceramics in the CaO–MgO–SiO2–P2O5 system, Ceram. Int. 38 (2012) 6677–6684.
[13] A. Moghanian, A. Sedghi, A. Ghorbanoghli, E. Salari, The effect of magnesium content on in vitro bioactivity, biological behavior and antibacterial activity of sol–gel derived 58S bioactive glass, Ceram. Int. (2018).
[14] A. M. El-Kady, A. F. Ali, R. A. Rizk, M. M. Ahmed, Synthesis, characterization and microbiological response of silver doped bioactive glass nanoparticles, Ceram. Int. 38 (2012) 177–188.
[15] C. Wu, Y. Zhou, M. Xu, P. Han, L. Chen, J. Chang, Y. Xiao, Copper-containing mesoporous bioactive glass scaffolds with multifunctional properties of angiogenesis capacity, osteostimulation and antibacterial activity, Biomaterials. 34 (2013) 422–433.
[16] R. L. Du, J. Chang, S. Y. Ni, W. Y. Zhai, J. Y. Wang, Characterization and in vitro Bioactivity of Zinc-containing Bioactive Glass and Glass-ceramics, J. Biomater. Appl. 20 (2006) 341–360.
[17] N. Kilcup, U. Werner-Zwanziger, E. Tonkopi, D. Boyd, Unanticipated stabilization of zinc-silicate glasses by addition of lanthanum:

Implications for therapeutic inorganic ion delivery systems, J. Non. Cryst. Solids. 429 (2015) 83–92.
[18] J. Ma, C. Z. Chen, D. G. Wang, J. H. Hu, Synthesis, characterization and in vitro bioactivity of magnesium-doped sol–gel glass and glass-ceramics, Ceram. Int. 37 (2011) 1637–1644.
[19] A. Hoppe, B. Sarker, R. Detsch, N. Hild, D. Mohn, W. J. Stark, A. R. Boccaccini, In vitro reactivity of Sr-containing bioactive glass (type 1393) nanoparticles, J. Non. Cryst. Solids. 387 (2014) 41–46.
[20] F. Baino, G. Novajra, V. Miguez-Pacheco, C. Vitale-Brovarone, Bioactive glasses: Special applications outside the skeletal system, J. Non. Cryst. Solids. 432 (2016) 15–30.
[21] M. E. Maguire, J. A. Cowan, Magnesium chemistry and biochemistry, BioMetals. 15 (2002) 203–210.
[22] D. H. H. M. Viering, J. H. F. de Baaij, S. B. Walsh, R. Kleta, D. Bockenhauer, Genetic causes of hypomagnesemia, a clinical overview, Pediatr. Nephrol. 32 (2017) 1123–1135.
[23] S. Castiglioni, A. Cazzaniga, W. Albisetti, J. Maier, Magnesium and Osteoporosis: Current State of Knowledge and Future Research Directions, Nutrients. 5 (2013) 3022–3033.
[24] M. M. Belluci, T. Schoenmaker, C. Rossa-Junior, S. R. Orrico, T. J. de Vries, V. Everts, Magnesium deficiency results in an increased formation of osteoclasts, J. Nutr. Biochem. 24 (2013) 1488–1498.
[25] S. Bernick, G. F. Hungerford, Effect of Dietary Magnesium Deficiency on the Bones and Teeth of Rats, J. Dent. Res. 44 (1965) 1317–1324.
[26] R. K. Rude, H. E. Gruber, L. Y. Wei, A. Frausto, B. G. Mills, Magnesium Deficiency: Effect on Bone and Mineral Metabolism in the Mouse, Calcif. Tissue Int. 72 (2003) 32–41.
[27] M. A. Saghiri, A. Asatourian, J. Orangi, C. M. Sorenson, N. Sheibani, Functional role of inorganic trace elements in angiogenesis—Part II: Cr, Si, Zn, Cu, and S, Crit. Rev. Oncol. Hematol. 96 (2015) 143–155.
[28] A. Nasulewicz, A. Mazur, A. Opolski, Role of copper in tumour angiogenesis—clinical implications, J. Trace Elem. Med. Biol. 18 (2004) 1–8.
[29] G. Hu, Copper stimulates proliferation of human endothelial cells under culture, J. Cell. Biochem. 69 (1998) 326–335.
[30] J. Li, D. Zhai, F. Lv, Q. Yu, H. Ma, J. Yin, Z. Yi, M. Liu, Preparation of copper-containing bioactive glass/eggshell membrane nanocomposites for improving angiogenesis, antibacterial activity and wound healing, Acta Biomater. (2016).
[31] J. Ye, J. He, C. Wang, K. Yao, Z. Gou, Copper-containing mesoporous bioactive glass coatings on orbital implants for improving drug delivery capacity and antibacterial activity, Biotechnol. Lett. 36 (2014) 961–968.
[32] J. Pérez-Pariente, A. F. Balas, M. Vallet-Regí*, Surface and Chemical Study of SiO2·P2O5·CaO·(MgO) Bioactive Glasses, Chem. Mater. 12 (2000) 750–755.
[33] J. Ma, C. Z. Chen, D. G. Wang, Y. Jiao, J. Z. Shi, Effect of magnesia on the degradability and bioactivity of sol–gel derived SiO2–CaO–MgO–P2O5 system glasses, Colloids Surfaces B Biointerfaces. 81 (2010) 87–95.
[34] M. Vallet-Regí, A. J. Salinas, J. Román, M. Gil, L. L. Hench, Effect of magnesium content on the in vitro bioactivity of CaO-MgO-SiO2-P2O5 sol-gel glasses, J. Mater. Chem. 9 (1999) 515–518.
[35] E. Dietrich, H. Oudadesse, In vitro bioactivity of melt-derived glass 46S6 doped with magnesium, J. Biomed. 88 (2009) 1087–1096.
[36] D. Bellucci, A. Sola, R. Salvatori, A. Anesi, L. Chiarini, V. Cannillo, Role of magnesium oxide and strontium oxide as modifiers in silicate-based bioactive glasses: Effects on thermal behaviour, mechanical properties and in-vitro bioactivity, Mater. Sci. Eng. C. 72 (2017) 566–575.
[37] S. J. Watts, R. G. Hill, M. D. O'Donnell, R. V. Law, Influence of magnesia on the structure and properties of bioactive glasses, J. Non. Cryst. Solids. 356 (2010) 517–524.
[38] M. Prabhu, K. Kavitha, P. Manivasakan, V. Rajendran, P. Kulandaivelu, Synthesis, characterization and biological response of magnesium-substituted nanobioactive glass particles for biomedical applications, Ceram. Int. 39 (2013) 1683–1694.
[39] M. Erol, A. Özyuguran, Ö. Çelebican, Synthesis, Characterization, and In Vitro Bioactivity of Sol-Gel-Derived Zn, Mg, and Zn-Mg Co-Doped Bioactive Glasses, Chem. Eng. Technol. 33 (2010) 1066–1074.
[40] J. S. Moya, A. P. Tomsia, A. Pazo, C. Santos, F. Guitin, In vitro formation of hydroxylapatite layer in a MgO-containing glass, J. Mater. Sci. Mater. Med. 5 (1994) 529–532.
[41] A.. Salinas, J. Román, M. Vallet-Regi, J. Oliveira, R.. Correia, M.. Fernandes, In vitro bioactivity of glass and glass-ceramics of the 3CaO·P2O5–CaO·SiO2–CaO·MgO·2SiO2 system, Biomaterials. 21 (2000) 251–257.
[42] A. Saboori, M. Rabiee, F. Moztarzadeh, M. Sheikhi, M. Tahriri, M. Karimi, Synthesis, characterization and in vitro bioactivity of sol-gel-derived SiO2–CaO–P2O5–MgO bioglass, Mater. Sci. Eng. C. 29 (2009) 335–340.
[43] X. Wang, X. Li, A. Ito, Y. Sogo, Synthesis and characterization of hierarchically macroporous and mesoporous CaO–MO–SiO2–P2O5 (M=Mg, Zn, Sr) bioactive glass scaffolds, Acta Biomater. 7 (2011) 3638–3644.
[44] A. Balamurugan, G. Balossier, J. Michel, S. Kannan, H. Benhayoune, A.H.S. Rebelo, J.M.F. Ferreira, Sol gel derived SiO2-CaO-MgO-P2O5 bioglass system—Preparation andin vitro characterization, J. Biomed. Mater. Res. Part B Appl. Biomater. 83B (2007) 546–553.
[45] R. Namba, M. Inacio, E. Paxton, Risk factors associated with deep surgical site infections after primary total knee arthroplasty: an analysis of 56,216 knees, JBJS. (2013).
[46] K. Yuan, Y. Chan, K. Kung, Comparison of osseointegration on various implant surfaces after bacterial contamination and cleaning: a rabbit study., Int. J. (2014).
[47] J. Kolmas, E. Groszyk, D. Kwiatkowska-Różycka, Substituted hydroxyapatites with antibacterial properties., Biomed Res. Int. 2014 (2014) 178123.
[48] D. Campoccia, L. Montanaro, C. R. Arciola, A review of the biomaterials technologies for infection-resistant surfaces, Biomaterials. 34 (2013) 8533–8554.
[49] T. Kokubo, H. Kushitani, S. Sakka, T. Kitsugi, T. Yamamuro, Solutions able to reproducein vivo surface-structure changes in bioactive glass-ceramic A-W3, J. Biomed. Mater. Res. 24 (1990) 721–734.
[50] H. M. Elgendy, M. E. Norman, A. R. Keaton, C. T. Laurencin, Osteoblast-like cell (MC3T3-E1) proliferation on bioerodible polymers: an approach towards the development of a bone-bioerodible polymer composite material, Biomaterials. 14 (1993) 263–269.
[51] Y. Gotoh, K. Hiraiwa, M. Nagayama, In vitro mineralization of osteoblastic cells derived from human bone., Bone Miner. 8 (1990) 239–50.
[52] C. E. Yellowley, Z. Li, Z. Zhou, C. R. Jacobs, H. J. Donahue, Functional Gap Junctions Between Osteocytic and Osteoblastic Cells, J. Bone Miner. Res. 15 (2010) 209–217.
[53] S. Hu, J. Chang, M. Liu, C. Ning, Study on antibacterial effect of 45S5 Bioglass®, J. Mater. Sci. Mater. Med. 20 (2009) 281–286.
[54] S. Hu, C. Ning, Y. Zhou, L. Chen, K. Lin, J. Chang, Antibacterial activity of silicate bioceramics, J. Wuhan Univ. Technol. Sci. Ed. 26 (2011) 226–230.
[55] R. L. Siqueira, O. Peitl, E. D. Zanotto, Gel-derived SiO2–CaO–Na2O–P2O5 bioactive powders: Synthesis and in vitro bioactivity, Mater. Sci. Eng. C. 31 (2011) 983–991.
[56] D. Xiao, Z. Tan, Y. Fu, K. Duan, X. Zheng, X. Lu, Hydrothermal synthesis of hollow hydroxyapatite microspheres with nano-structured surface assisted by inositol hexakisphosphate, Ceram. Int. (2014).
[57] M. Mozafari, F. Moztarzadeh, M. Tahriri, Investigation of the physico-chemical reactivity of a mesoporous bioactive SiO2–CaO–P2O5 glass in simulated body fluid, J. Non. Cryst. Solids. 356 (2010) 1470–1478.
[58] R. Kamalian, A. Yazdanpanah, F. Moztarzadeh, R. Ravarian, Z. Moztarzadeh, M. Tahmasbi, # Masoud Mozafari, Synthesis And Characterization Of Bioactive Glass/Forsterite Nanocomposites For Bone Implants, Ceram. – Silikáty. 56 (2012) 331–340.
[59] V. K. Vyas, A. S. Kumar, S. Prasad, S. P. Singh, R. Pyare, Bioactivity and mechanical behaviour of cobalt oxide-doped bioactive glass, Bull. Mater. Sci. 38 (2015) 957–964.
[60] K. Zhang, H. Yan, D.C. Bell, A. Stein, L. F. Francis, Effects of materials parameters on mineralization and degradation of sol-gel bioactive glasses with 3D-ordered macroporous structures, J. Biomed. Mater. Res. 66A (2003) 860–869.
[61] L. L. Hench, J. Wilson, An Introduction to Bioceramics, World Scientific, 1993.
[62] J. R. Jones, New trends in bioactive scaffolds: The importance of nanostructure, J. Eur. Ceram. Soc. 29 (2009) 1275–1281.
[63] X. Chen, J. Ou, Y. Wei, Z. Huang, Y. Kang, G. Yin, Effect of MgO contents on the mechanical properties and biological performances of bioceramics in the MgO–CaO–SiO2 system, J. Mater. Sci. Mater. Med. 21 (2010) 1463–1471.
[64] D. Khvostenko, T. J. Hilton, J. L. Ferracane, J. C. Mitchell, J. J. Kruzic, Bioactive glass fillers reduce bacterial penetration into marginal gaps for composite restorations, Dent. Mater. 32 (2016) 73–81.
[65] J. P. Ruparelia, A. K. Chatterjee, S. P. Duttagupta, S. Mukherji, Strain

specificity in antimicrobial activity of silver and copper nanoparticles, Acta Biomater. 4 (2008) 707–716.
[66] Robinson D Griffith R Shechtman D Evans R Conzemius M, In vitro antibacterial properties of magnesium metal against Escherichia coli, Pseudomonas aeruginosa and Staphylococcus aureus, Acta Biomater. 6 (2010) 1869–1877.
[67] I. Allan, H. Newman, M. Wilson, Antibacterial activity of particulate Bioglass® against supra- and subgingival bacteria, Biomaterials. 22 (2001) 1683–1687.
[68] M. Kazem-Rostami, A. Moghanian, Hünlich base derivatives as photo-responsive Λ-shaped hinges, Org. Chem. Front. 4 (2017) 224–228.
[69] A. Khazaei, S. Saednia, J. Saien, M. Kazem-Rostami, M. Sadeghpour, M. K. Borazjani, F. Abbasi, Grafting Amino Drugs to Poly(styrene- *alt* -maleic Anhydride) as a Potential Method for Drug Release, J. Braz. Chem. Soc. 24 (2013) 1109–1115.